RAA 2021 Vol. **21** No. **11**, 287(12pp) doi: 10.1088/1674-14527/21/11/287

http://www.raa-journal.org *http://iopscience.iop.org/raa*

***R**esearch in*
***A**stronomy and*
***A**strophysics*

Iron group nuclei electron capture in super-Chandrasekhar superstrong magnetic white dwarfs

Jing-Jing Liu and Dong-Mei Liu

College of Science, Hainan Tropical Ocean University, Sanya 572022, China; *liujingjing68@126.com*

Received 2021 May 8; accepted 2021 July 27

Abstract Using the theory of relativistic mean-field effective interactions, the influences of superstrong magnetic fields (SMFs) on electron Fermi energy, binding energy per nucleus and single-particle level structure are discussed in super-Chandrasekhar magnetic white dwarfs. Based on the relativistical SMFs theory model of Potekhin et al., the electron chemical potential is corrected in SMFs, and the electron capture (EC) of iron group nuclei is investigated by using the Shell-Model Monte Carlo method and Random Phase Approximation theory. The EC rates can increase by more than three orders of magnitude due to the increase of the electron Fermi energy and the change of single-particle level structure by SMFs. However, the EC rates can decrease by more than four orders of magnitude due to increase of the nuclei binding energy by SMFs. We compare our results with those of FFNs (Fuller et al.), AUFDs (Aufderheide et al.) and Nabi (Nabi et al.). Our rates are higher by about four orders of magnitude than those of FFN, AUFD and Nabi due to SMFs. Our study may have important reference value for subsequent studies of the instability, mass radius relationship, and thermal and magnetic evolution of super-Chandrasekhar magnetic white dwarfs.

Key words: nuclear reactions, nucleosynthesis, abundances — stars: white dwarfs

1 INTRODUCTION

In the early stage of the core collapse of a massive star, an important aspect that the maximum possible mass of non-rotating, non-magnetized white dwarfs (WDs) is $1.44\,M_{\odot}$ was demonstrated by Chandrasekhar (Chandrasekhar 1935). However, the discovery of some over-luminous type Ia supernovae (SNeIa) such as SN 2006gz, SN 2007if, SN 2009dc and SN 2003fg highlighted peculiar, anomalous observations (Scalzo et al. 2010). These particular SNeIa may derive from the explosions of rapidly rotating WDs or from the mergers of two massive WDs. They have been observed with exceptionally higher luminosities but lower kinetic energies. Their mass of the exploding WDs (progenitors of supernovae) may be between $2.1 \sim 2.8\,M_{\odot}$, significantly super-Chandrasekhar. This characteristic seemed not to abide by the Chandrasekhar limit. The progenitors of these SNeIa are called highly super-Chandrasekhar WDs by some astrophysicists (Das & Mukhopadhyay 2012a,b; Das et al. 2013).

Recently, some works suggested that super-luminous SNeIa could be derived from the explosions of strongly magnetized WDs (Das & Mukhopadhyay 2012a,b; Das et al. 2013; Das & Mukhopadhyay 2013; Kundu & Mukhopadhyay 2012). In the presence of a strongly quantizing magnetic field, the equation of state of dense matter becomes so stiff that the electron degeneracy pressure may be high enough to support WDs with masses up to $\sim 2.6\,M_{\odot}$.

Some magnetized WDs have been discovered with surface fields of 10^8 G to 10^{13} G (Kemp et al. 1970; Schmidt & Smith 1995; Reimers et al. 1996). Some works considered that highly super-Chandrasekhar WDs could have interior magnetic fields of $\geq 10^{15}$ G (Das & Mukhopadhyay 2012a,b; Das et al. 2013). High magnetic field strength will modify the equation of state of the degenerate matter by causing Landau quantization of the electrons. Some investigations revealed that the weak interaction processes (e.g., electron capture (EC) and beta decay) play a decisive role in super-Chandrasekhar magnetic WDs (SCMWDs) (Chamel et al. 2013).

ECs on nuclei in the iron mass region will start after the core mass exceeds the Chandrasekhar mass limit, reducing the electron pressure, and thus accelerating the collapse. They also lower the electron to baryon ratio, which leads to a supernova explosion. By applying the parameterization of the Gamow-Teller (GT) strength distribution for nuclei, Fuller et al. (1980), Fuller et al. (1982), Fuller et al. (1985) (hereafter FFN) investigated

the EC rates and did some pioneering works in the study of supernovae. The EC rates of iron group nuclei also have been discussed by some authors (e.g., Dean et al. (1998); Aufderheide et al. (1990); Aufderheide et al. (1994) (hereafter AUFD); Langanke & Martinez-Pinedo (1998); Langanke & Martínez-Pinedo (2000), Liu (2013); Liu et al. (2017a); Liu & Liu (2018b). Gao et al. (2011); Gao et al. (2015); Li et al. (2016); Gao et al. (2017)) who also investigated the electron Fermi energy and electron fraction in a neutron star and the effects of superhigh magnetic fields on the equation of state. However, they neglected the effect of a superstrong magnetic field (hereafter SMF) on EC.

The weak interaction reactions and neutrino energy loss on iron group nuclei had been discussed by considering the quantum effect in SMFs in our previous works (e.g., Liu (2014); Liu & Liu (2016); Liu & Gu (2016); Liu (2016); Liu et al. (2016); Liu et al. (2017b)). For neutron stars, Dai et al. (1993); Luo & Peng (1997) discussed the influence of SMFs on EC, which only focused on the effect of the ground state transition at zero temperature and ignored that of the GT transition. Some recent studies (Liu & Liu 2016; Liu & Gu 2016; Liu 2016; Lai & Shapiro 1991; Lai 2001) reported that a wide-range for the equation of state and electron Fermi energy is needed for calculations of the structure and weak interaction in SMFs.

The SMFs strongly affect the equation of state of the material. For example, the electron degeneracy equation of state can be corrected by the magnetic field due to the strong quantization of Landau levels. SMFs also deeply affect the structure of SCMWDs. When the internal magnetic field intensity is considered to reach 10^{18} G, the mass limit of SCMWDs may be increased to $2.58\,M_{\odot}$ (see Das & Mukhopadhyay 2012a,b; Das et al. (2013)). The influences of SMFs, virial theorem, gravitational and dynamic instability, the breaking of spherical symmetry, general relativity effect, EC and thermonuclear reaction of super-dense matter will introduce new and severe challenges to the study of mass limit, stability and neutrino cooling of SCMWDs.

In the present paper, based on the SMFs model in a neutron star (Potekhin & Chabrier 2013; Potekhin et al. 2013; Potekhin & Chabrier 2018) and the relativistic mean-field effective interactions theory (Lalazissis et al. 1997; Lalazissis et al. 2005), we will discuss the effect of SMFs on electron Fermi energy, binding energy per nucleus and single-particle level structure in SCMWDs. Based on the Shell-Model Monte Carlo (SMMC) method (Dean et al. 1998; Juodagalvis et al. 2010), and the random phase approximation (RPA) theory, we discuss the EC reaction of iron group nuclei. Our calculations may be universal, very important and helpful for the studies of SCMWDs. We compare our results in SMFs with those of FFN, AUFD and Nabi & Klapdor-Kleingrothaus (1999) (hereafter NKK) in non-SMFs. Our discussions also differ from our previous studies (Liu & Liu 2018b), which analyzed the EC by applying the method of Brink hypothesis in the crust of neutron stars.

The present paper is organized as follows. In the next section, we analyze the effect of SMFs on the matter in SCMWDs. The EC rates in and not in SMFs are discussed in Section 3. Some numerical results and discussions are given in Section 4. Finally, some conclusions are summarized in Section 5.

2 THE EFFECT OF SMFS ON THE MATTER IN SCMWDS

2.1 The Effect of SMFs on the Nuclear Energy

In SCMWDs, the atoms are completely ionized. For a uniform relativistic electron Fermi gas, the Gibbs free energy per baryon $g(A, Z, P)$ for a Coulomb lattice is

$$g(A, Z, P) = \frac{E(A, Z, P) + PV}{A} = \varepsilon + \frac{P}{n}, \quad (1)$$

where ε, $n = A/V$ and V are the corresponding energy per nucleon, the baryon density in a cell and the volume occupied by a unit cell of the Coulomb lattice, respectively.

The energy per nucleon ε consists of three different contributions from nuclear, electronic and lattice, and is given by

$$\varepsilon = \varepsilon_n(A, Z) + \varepsilon_e(A, Z, P) + \varepsilon_l(A, Z, n), \quad (2)$$

where

$$\varepsilon_n(A, Z) = \frac{M(A, Z)}{A} = \frac{1}{A}[zm_p + (A-Z)m_n - \varepsilon_{\rm bind}(A, Z)], \quad (3)$$

$$\varepsilon_e(A, Z, P) = \frac{1}{n\pi^2}\int_0^{p_F} p^2\sqrt{p^2 + m_e^2c^4}dp, \quad (4)$$

$$\varepsilon_l(A, Z, n) = -1.81962\frac{(Ze)^2}{a} = -C_{\rm bcc}\frac{Z^2}{A^{4/3}}p_F. \quad (5)$$

Here $\varepsilon_n(A, Z)$ is the nuclear contribution to the total energy per nucleon. $\varepsilon_e(A, Z, P)$ is the electronic contribution for a degenerate free Fermi gas and $\varepsilon_l(A, Z, n)$ is the lattice energy per baryon. $C_{\rm bcc} = 3.40665 \times 10^{-3}$ and a is the lattice constant (Shapiro & Teukolsky 1983). $M(A, z)$, $\varepsilon_{\rm bind}(A, Z)$, m_n and m_p are the nuclear mass, binding energy, and neutron and proton masses, respectively.

The influences of SMFs on the nuclear binding energy had been discussed based on the relativistic mean-field effective interactions theory of NL3 (Lalazissis et al. 1997) and DD-ME2 (Lalazissis et al. 2005; Peña Arteaga et al.

2011). According to a covariant density functional, an effective Lagrangian with nucleons and mesons is expressed as (e.g., Gambhir et al. 1990; Vretenar et al. 2005)

$$L = L_N + L_m + L_{\rm int} + L_{\rm BO} + L_{\rm BM}, \quad (6)$$

where L_N, L_m and $L_{\rm int}$ are the Lagrangian of the free nucleon, the free meson fields and the electromagnetic field generated by the proton, and the Lagrangian describing the interactions, respectively. According to Bjorken et al. (1965), we can express the coupling of the proton orbital motion with the external magnetic field, and the coupling of proton and neutron intrinsic dipole magnetic moments with the external magnetic field as $L_{\rm BO}$ and $L_{\rm BM}$, respectively.

2.2 The Effect of SMFs on the Electron Properties

In SCMWDs, the global structure of a WD is determined by the equation of state, which relates the pressure and mass density. The SMFs significantly modify the matter equation of state, electron energy, and the structure and composition of SCMWDs. The energy eigenstate of an electron must obey the relativistic Dirac equation and is written as (e.g., Potekhin & Chabrier 2013; Potekhin et al. 2013; Potekhin & Chabrier 2018)

$$\begin{aligned} E_n = \varepsilon_n^B &= [c^2 p_z^2 + m_e^2 c^4 (1 + 2\nu \frac{B}{B_{cr}})]^{1/2} \\ &= [c^2 p_z^2 + m_e^2 c^4 (1 + 2\nu b)]^{1/2}, \end{aligned} \quad (7)$$

where $\nu = n_l + (1+\sigma_z)/2$. $\sigma_z = -1$ and $\sigma_z = \pm 1$ are the spin degeneracies for the ground Landau level ($n_l = 0$) and excited levels, respectively; $b = B/B_{\rm cr}, B_{\rm cr} = m_e^2 c^3/e\hbar = 4.414 \times 10^3$ G. The transverse motion of the electron becomes relativistic when $\hbar\omega_c \geq m_e c^2$ (i.e. $B \geq B_{\rm cr}$) for extremely strong magnetic fields. The maximum number of Landau levels $\nu_{\rm max}$, related to the highest value of the allowed interaction energy, should be satisfied with $E_n(\nu_{\rm max}, p_z = 0) = U_e$. So, we have

$$\nu_{\rm max} = \frac{1}{2b}(\frac{U_e^2}{m_e^2 c^4} - 1). \quad (8)$$

According to the discussions by Potekhin & Chabrier (2013); Potekhin et al. (2013); Potekhin & Chabrier (2018) on SMFs at the crust of a neutron star, one can express the electron number density n_e and the pressure in a relativistic magnetic field as

$$n_e^B = \frac{1}{\pi^{3/2} a_m^2 \lambda_e} \sum_{n=0}^{\infty} \sum_{\sigma} (1+2nb)^{1/4} \frac{\partial I_{1/2}(\chi_n, \tau_n)}{\partial \chi_n} \quad (9)$$

$$P_e = \frac{kT}{\pi^{3/2} a_m^2 \lambda_e} \sum_{n=0}^{\infty} \sum_{\sigma} (1+2nb)^{1/4} I_{1/2}(\chi_n, \tau_n) \quad (10)$$

where $\lambda_e = (2\pi\hbar^2/m_e kT)^{1/2}$ is the thermal de Broglie wavelengths of free electrons and $a_m = (\hbar c/eB)^{1/2}$ is the magnetic length, which yields a characteristic transverse scale of the electron wave function. $\tau_n = \tau/\sqrt{1+2nb}$ and $\chi_n = \chi_e + \tau^{-1} - \tau_n^{-1}$, where $\chi_e = U_F^B/kT, \tau = T/T_r$ (here U_F^B is electron chemical potential without rest energy $m_e c^2$ in no SMFs, $T_r = m_e c^2/k = 5.93 \times 10^9$ K and $I_\nu(\chi_e, \tau) \equiv \int_0^\infty x^\nu (1+\tau x/2)^{1/2}/(\exp(x-\chi_e)+1) dx$).

According to Blinnikov et al. (1996); Girifalco (1973), $I_\nu(\chi_e, \tau)$ is

$$I_\nu(\chi_e, \tau) = \frac{1}{\sqrt{2}\tau^{\nu+1}} (I_\nu^{(0)}(\tilde{\mu}) + \frac{\pi^2\tau^2}{6} I_\nu^{(2)}(\tilde{\mu}) + ...), \quad (11)$$

where $\tilde{\mu} = \chi_e \tau = U_F^B/m_e c^2$ is the electron chemical potential (without the rest energy) in relativistic units,

By conditions of $\rho < \rho_B = 7054(A/z) B_{12}^{3/2} {\rm g\,cm^{-3}}$ and $T < T_F = \hbar\omega_c/k = 1.3434 \times 10^8 B_{12}/\gamma_r$ K (here $\gamma_r = \sqrt{1+x_r}, x_r = (10\rho_7 z/A)^{1/3}$), the magnetic field will be strongly quantized and the electrons are strongly degenerate. Therefore, based on Equations (7) and (9), the Fermi energy ϵ_F is determined by

$$n_e^B = \frac{m_e c}{\hbar} \frac{b}{2\pi^2} \sum_{n=0}^{\infty} \sum_{\sigma} (1+2nb)^{1/2} I_{1/2}^{(1)}(\tilde{\epsilon_n}), \quad (12)$$

where $\tilde{\epsilon_n} = \epsilon_F/m_e c^2 + 1 - \sqrt{1+2nb}$, the chemical potential is given by $U_F^B = \epsilon_F + \Delta\epsilon$ and $\Delta\tilde{\epsilon} = \Delta\epsilon/m_e c^2$. According to Potekhin & Chabrier (2013); Potekhin et al. (2013); Potekhin & Chabrier (2018), we have

$$\Delta\tilde{\epsilon} = -\frac{\pi^2\tau^2}{6} \frac{\sum_{n=0}^{\infty} \sum_{\sigma} (1+2nb)^{1/2} I_{1/2}^{(3)}(\tilde{\epsilon_n})}{\sum_{n=0}^{\infty} \sum_{\sigma} (1+2nb)^{1/2} I_{1/2}^{(2)}(\tilde{\epsilon_n})}, \quad (13)$$

where

$$I_\nu^{(n+1)}(\tilde{\mu}) = \frac{dI_\nu^{(n)}}{d\tilde{\mu}}, \quad (14)$$

$$I_{1/2}^0(\tilde{\mu}) = [\tilde{x}\tilde{y} - \ln(\tilde{x} + \tilde{y})]/2, \quad (15)$$

$$I_{3/2}^0(\tilde{\mu}) = \tilde{x}^3/3 + I_{1/2}^0(\tilde{\mu}), \quad (16)$$

$$I_{5/2}^0(\tilde{\mu}) = \tilde{x}^3\tilde{y}/4 - 2\tilde{x}^3/3 + 1.25 I_{1/2}^0(\tilde{\mu}), \quad (17)$$

here $\tilde{x} = \sqrt{\tilde{\mu} + 2\tilde{\mu}}$, $\tilde{y} = 1 + \tilde{\mu}$. According to Equations (17), (18), we have

$$\begin{aligned} I_{1/2}^{(1)}(\tilde{\epsilon_n}) &= (\tilde{\epsilon_n} + 1)(\tilde{\epsilon_n}^2 + 2\tilde{\epsilon_n})^{-1/2} \\ &+ (2\tilde{\epsilon_n}^3 + 3\tilde{\epsilon_n}^2)(\tilde{\epsilon_n}^4 + 2\tilde{\epsilon_n^3})^{-1/2} \\ &+ \frac{(\tilde{\epsilon_n} + 1)(\tilde{\epsilon_n}^2 + 2\tilde{\epsilon_n})^{-1/2}}{2(1 + \tilde{\epsilon_n} + \sqrt{\tilde{\epsilon_n}^2 + 2\tilde{\epsilon_n}})}. \end{aligned} \quad (18)$$

According to Equations (12), (13), (16), we can also derive the results of $I_{1/2}^{(3)}(\tilde{\epsilon_n})$ and $I_{1/2}^{(2)}(\tilde{\epsilon_n})$. When the higher order terms are negligible in Equation (11), we have

(see Potekhin & Chabrier (2013); Potekhin et al. (2013); Potekhin & Chabrier (2018) and reference therein)

$$\Delta\tilde{\epsilon} = -\frac{\pi^2\tau^2}{6x_B^2(1+x_B^2)^{1/2}}, \tag{19}$$

where $x_B \approx 302z\rho_7/AB_{12}$ (ρ_7 is density in the unit of $10^7\,\mathrm{g\,cm^{-3}}$).

3 THE STUDY OF EC

Based on RPA theory, the EC rates related to the capture cross section is (Dean et al. 1998; Langanke & Martinez-Pinedo 1998; Langanke & Martínez-Pinedo 2000; Juodagalvis et al. 2010)

$$\lambda_{if} = \frac{1}{\pi^2\hbar^3}\sum_{if}\int_{\varepsilon_0}^{\infty} p_e^2\sigma_{\mathrm{ec}}(\varepsilon_e,\varepsilon_i,\varepsilon_f)f d\varepsilon_n \tag{20}$$

where $\varepsilon_0 = \max(Q_{if},1)$. $p_e = \sqrt{\varepsilon_e - 1}$ is the momentum of the incoming electron with energy ε_e. $f = [1+\exp(\varepsilon_e - U_F/kT)]^{-1}$ and σ_{ec} are the electron Fermi-Dirac distribution and the capture cross section. U_F is the electron chemical potential, and k and T are the Boltzmann constant and the electron temperature, respectively. (Note that in this paper all of the energies and the momentums are respectively in units of m_ec^2 and m_ec, where m_e is the electron mass and c is the speed of light in a vacuum.)

According to energy conservation from the electron, proton and neutron energies, and the neutrino energy, EC Q-value is (Langanke & Martinez-Pinedo 1998; Langanke & Martínez-Pinedo 2000)

$$Q_{i,f} = \varepsilon_e - \varepsilon_\nu = \varepsilon_f^n - \varepsilon_i^p = \varepsilon_{if}^* + \hat{\mu} + \Delta_{np} \tag{21}$$

where ε_i is the energy of an initial proton single particle state, and ε_f is the energy of a neutron single particle state. $\hat{\mu} = \mu_n - \mu_p$ and $\Delta_{np} = M_nc^2 - M_pc^2 = 1.293\,\mathrm{MeV}$ are the chemical potential difference and the mass difference between neutron and proton, respectively. $Q_{00} = M_fc^2 - M_ic^2 = \hat{\mu} + \Delta_{np}$, with M_i and M_f being the masses of the parent nucleus and the daughter nucleus respectively; ε_{if}^* corresponds to the excitation energies in the daughter nucleus at the states with zero temperature.

The electron chemical potential U_F^0 in the case without SMFs is

$$n_e^0 = \rho Y_e N_A = \frac{8\pi}{(2\pi)^3}\int_0^{\infty} p_e^2(f_{-e} - f_{+e})dp_e \tag{22}$$

where N_A, Y_e and ρ are Avogadro constant, electron abundance and density in $\mathrm{g\,cm^{-3}}$, respectively. $f_{-e} = [1+\exp(\varepsilon_e - U_F^0/kT)]^{-1}$ and $f_{+e} = [1+\exp(\varepsilon_e + U_F^0/kT)]^{-1}$ are the electron and positron distribution functions, respectively.

According to the SMMC method, the total EC cross section is (Langanke & Martinez-Pinedo 1998; Langanke & Martínez-Pinedo 2000)

$$\begin{aligned}\sigma_{\mathrm{ec}} &= \sigma_{\mathrm{ec}}(\varepsilon_n) = \sum_{if}\frac{(2J_i+1)\exp(-\beta E_i)}{Z_A}\sigma_{fi}(\varepsilon_e)\\ &= 6g_{wk}^2\int d\xi(\varepsilon_e-\xi)^2\frac{G_A^2}{12\pi}S_{GT^+}(\xi)F(Z,\varepsilon_e),\end{aligned} \tag{23}$$

where $G_A = 1.25$, $g_{wk} = 1.1661\times10^{-5}\,\mathrm{GeV^{-2}}$ and $F(Z,\varepsilon_e)$ are the axial vector form factor at zero momentum, the weak coupling constant and the Coulomb wave correction, respectively. For an initial state, S_{GT^+} is the total amount of GT strength, which is calculated by summing over a complete set of final states in the GT transition matrix elements $|M_{GT}|_{if}^2$.

The SMMC method is also used to calculate the response function $R_A(\tau)$ of an operator $\hat{A}$ at an imaginary time τ. By utilizing a spectral distribution of initial and final states $|i\rangle$ and $|f\rangle$ with energies E_i and E_f respectively, $R_A(\tau)$ is expressed as (Dean et al. 1998; Langanke & Martínez-Pinedo 2000)

$$R_A(\tau) = \frac{\sum_{if}(2J_i+1)e^{-\beta E_i}e^{-\tau(E_f-E_i)}|\langle f|\hat{A}|i\rangle|^2}{\sum_i(2J_i+1)e^{-\beta E_i}}. \tag{24}$$

Note that the total strength for the operator is given by $R(\tau=0)$. The strength distribution is expressed as

$$\begin{aligned}S_{GT^+}(\varepsilon) &= \frac{\sum_{if}\delta(\varepsilon - E_f + E_i)(2J_i+1)e^{-\beta E_i}|\langle f|\hat{A}|i\rangle|^2}{\sum_i(2J_i+1)e^{-\beta E_i}}\\ &= S_A(\varepsilon),\end{aligned} \tag{25}$$

where the strength distribution $S_{GT^+}(\varepsilon)$ is related to $R_A(\tau)$ by a Laplace Transform. E is the energy transfer within the parent nucleus in units of $\mathrm{MeV^{-1}}$, $\beta = 1/T_N$ and T_N is the nuclear temperature.

According to the expression of the EC rate Equation (20) in the case without SMFs, we can derive a formula for EC rates in SMFs from one of the initial states to all possible final states. We can reference equations (20)-(23) in Liu & Liu (2018a). It is given by

$$\lambda_{\mathrm{ec}}^{\mathrm{B}}(\mathrm{LJ}) = \frac{\ln 2}{6163}\int_0^{\infty}\mathrm{d}\xi\mathrm{S}_{\mathrm{GT}}^{\mathrm{B}}\frac{\mathrm{c}^3}{(\mathrm{m_ec^2})^5}\mathrm{f}_{\mathrm{if}}^{\mathrm{B}}. \tag{26}$$

The total EC cross section in SMFs is expressed as

$$\begin{aligned}\sigma_{\mathrm{ec}}(\varepsilon_n^B) &= \sum_{if}\frac{(2J_i+1)\exp(-\beta E_i)}{Z_A}\sigma_{fi}(\varepsilon_e^B)\\ &= 6g_{wk}^2\int d\xi(\varepsilon_e^B-\xi)^2\frac{G_A^2}{12\pi}S_{GT^+}^B(\xi)F^B(Z,\varepsilon_e^B),\end{aligned} \tag{27}$$

where the strength distribution will change from $S_{GT^+}(\xi)$ to $S^B_{GT^+}(\xi)$ according to Equations (24), (25) and the phase space factor f^B_{if} in SMFs can be defined as

$$f^{\rm B}_{if} = \frac{c^3}{(m_e c^2)^5}\frac{b}{2}\sum_0^\infty \theta_n$$
$$= \frac{c^3}{(m_e c^2)^5}\frac{b}{2}\sum_0^\infty g_{no}\int_{p_0^B}^\infty dp_e p_e^2(-\xi+\varepsilon_n)^2 F^B(Z,\varepsilon_n^B) f\,. \quad (28)$$

Here $f = f(\varepsilon_n^B, U_F^B, T)$ is the electron Fermi-Dirac distribution, ε_n^B is the total rest mass and kinetic energies in an SMF; $F^B(Z,\varepsilon_n)$ is the Coulomb wave correction in SMFs.

The p_0^B is defined as

$$p_0^B = \begin{cases} \sqrt{Q_{if}^2 - \Theta}, & (Q_{if} < \Theta^{1/2}) \\ 0 & (\text{otherwise}), \end{cases} \quad (29)$$

where $\Theta = m_e^2c^4(1+2\nu B/B_{cr}) = m_e^2c^4(1+2\nu b)$.

The rate of change of electronic abundance (RCEA) is an important parameter in SCMWD evolution. It is given by

$$\dot{Y_e^{ec}}(k) = \frac{dY_e}{dt} = -\frac{X_k}{A_k}\lambda_k^{ec}, \quad (30)$$

where X_k is the mass fraction of the kth nucleus and A_k is the mass number of the kth nucleus.

4 RESULTS AND DISCUSSIONS

Figures 1–5 feature the EC rates of some iron group nuclei as a function of the magnetic field B at some typical astrophysical surroundings. One can find that when $10^{10}\,\mathrm{G} < \mathrm{B} < 10^{14}\,\mathrm{G}$ and at relatively low density and temperature (e.g., $\rho_7 < 5, T_9 < 1$) the magnetic field has a minor effect on the EC. However, the EC rates are influenced greatly at relatively high density (e.g., $\rho_7 \geq 5.86$). For example, the EC rates for some iron group nuclei (e.g., $^{52-61}$Fe, $^{55-60}$Co and $^{56-63}$Ni) increase no more than by one order of magnitude at $\rho_7 = 5.86, T_9 = 0.399$ and $\rho_7 = 4.99, T_9 = 0.877$ when $B < 10^{14}$ G, but increase greatly by more than three orders of magnitude at relatively high temperature and density when $B < 10^{14}$ G (e.g. for $^{55-60}$Co at $\rho_7 = 15.44, T_9 = 3.84$). (We note in this paper T_9, ρ_7 and B_{12} are the temperature, density and magnetic field in units of 10^9 K, $10^7\,\mathrm{g\,cm^{-3}}$ and 10^{12} G, respectively.)

Maeda et al. (2009) discussed Subaru and Keck observations of the peculiar SNIa 2006GZ at late phases. Their results affirm that SNeIa (e.g., SN Ia 2006GZ) exhibiting exceptionally large peak luminosity have been discovered. Their luminosity requires more than $1\,M_\odot$ of ^{56}Ni, which can be derived from the EC reaction of iron group nuclei which are ejected during the explosion, suggesting that they might have originated from super-Chandrasekhar mass WDs.

Table 1 Comparisons of the maximum value of our calculations $\lambda_{\rm ec}^B(\mathrm{LJ})$ with those of minimum value for some typical iron group nuclides in SMFs at $\rho_7 = 5.86, Y_e = 0.47, T_9 = 3.40$ for $10^{13}\,\mathrm{G} \leq B \leq 10^{16}\,\mathrm{G}$.

	$\rho_7 = 5.86, Y_e = 0.47, T_9 = 3.40$			
Nuclide	B	$\lambda^B_{\rm max}(\mathrm{LJ})$	B	$\lambda^B_{\rm min}(\mathrm{LJ})$
^{56}Ni	6.280e13	9.279e2	4.037e14	3.062e0
^{57}Ni	6.280e13	9.063e2	4.037e14	8.741e0
^{58}Ni	6.280e13	6.782e2	8.498e14	4.319e-2
^{59}Ni	6.280e13	6.299e2	4.037e14	1.679e0
^{60}Ni	5.214e13	4.772e2	1.024e15	6.090e-6
^{53}Fe	6.280e13	6.967e2	2.783e14	7.662e0
^{54}Fe	6.280e13	6.443e2	8.498e14	7.070e-2
^{55}Fe	5.214e13	6.419e2	1.024e15	1.065e-2
^{55}Co	6.28e13	1.020e3	4.037e14	7.396e0
^{56}Co	6.28e13	9.442e2	3.352e14	1.153e1
^{57}Co	6.28e13	7.330e2	3.857e14	5.193e-1
^{58}Co	5.214e13	7.370e2	3.352e14	3.118e0

Table 2 Comparisons of the maximum value of our calculations $\lambda_{\rm ec}^B(\mathrm{LJ})$ with those of minimum value for some typical iron group nuclides in SMFs at $\rho_7 = 14.5, Y_e = 0.45, T_9 = 3.80$ for $10^{13}\mathrm{G} \leq B \leq 10^{16}\,\mathrm{G}$.

	$\rho_7 = 14.5, Y_e = 0.45, T_9 = 3.80$			
Nuclide	B	$\lambda^B_{\rm max}(\mathrm{LJ})$	B	$\lambda^B_{\rm min}(\mathrm{LJ})$
^{57}Co	1.322e14	1.850e3	1.485e15	1.289e0
^{58}Co	1.322e14	1.869e3	1.024e15	7.851e0
^{59}Co	1.322e14	1.222e3	2.595e15	2.210e-3
^{60}Co	1.322e14	1.134e3	1.789e15	2.280e-1
^{55}Mn	1.322e14	1.370e3	2.154e15	8.339e-5
^{56}Mn	1.322e14	1.483e3	2.154e15	1.777e-3
^{55}Fe	1.322e14	1.627e3	2.154e15	1.909e-1
^{56}Fe	1.322e14	1.264e3	2.595e15	2.918e-6
^{57}Fe	1.322e14	1.291e3	2.595e15	1.322e-5
^{60}Ni	1.322e14	1.210e3	2.595e15	4.869e-3
^{61}Ni	1.322e14	1.686e3	2.595e15	1.336e1
^{53}Cr	1.322e14	1.256e3	2.154e15	6.325e-6

Table 3 Comparisons of the maximum value of our calculations $\lambda_{\rm ec}^B(\mathrm{LJ})$ with those of minimum value for some typical iron group nuclides in SMFs at $\rho_7 = 106, Y_e = 0.43, T_9 = 4.93$ for $10^{13}\,\mathrm{G} \leq B \leq 10^{17}\,\mathrm{G}$.

	$\rho_7 = 106, Y_e = 0.43, T_9 = 4.93$			
Nuclide	B	$\lambda^B_{\rm max}(\mathrm{LJ})$	B	$\lambda^B_{\rm min}(\mathrm{LJ})$
^{55}Mn	1.024e15	1.059e4	1.385e16	5.073e-3
^{56}Mn	1.024e15	1.104e4	1.668e16	5.205e-2
^{57}Mn	1.024e15	7.641e3	1.668e16	1.248e-5
^{58}Mn	8.498e14	4.836e3	1.668e16	1.805e-4
^{59}Fe	1.024e15	6.426e3	1.668e16	2.985e-6
^{61}Ni	1.024e15	6.236e3	1.668e16	1.165e-1
^{62}Ni	1.024e15	4.428e3	1.668e16	7.589e-6
^{63}Ni	1.024e15	4.275e3	1.668e16	3.910e-4

As the SMF increases, some change and difference from the curves are presented due to strong quantum effects. The higher the magnetic field, the larger the influence becomes. The lower the electron energy in SMFs is, the lower the Landau levels that will be occupied by electrons. However, the lower the magnetic fields and the higher the density, the higher the electron chemical potential becomes. At relatively high density, as

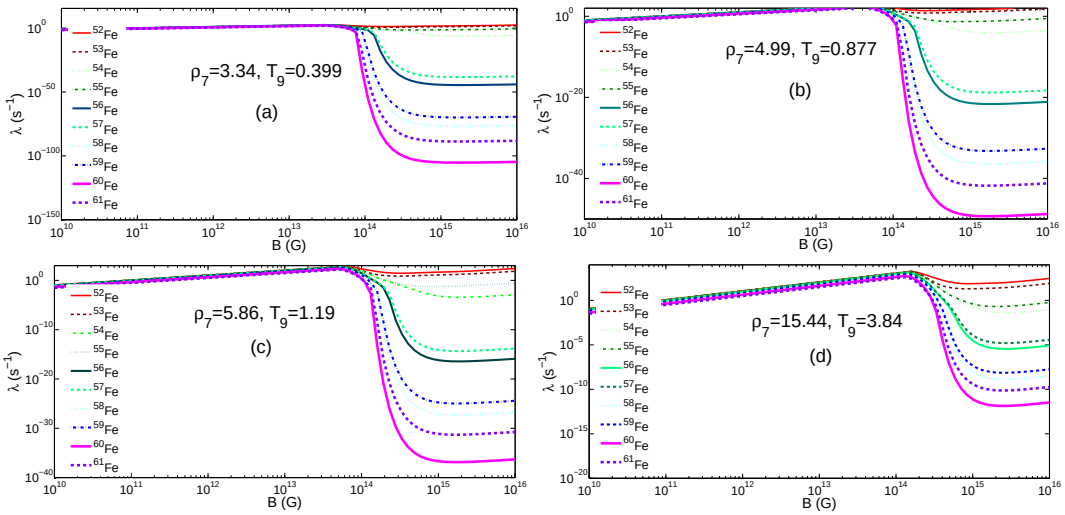

Fig. 1 The EC rates for $^{52-61}$ Fe as a function of the magnetic field at $\rho_7 = 3.34, T_9 = 0.399$; $\rho_7 = 4.99, T_9 = 0.877$; $\rho_7 = 5.86, T_9 = 1.19$ and $\rho_7 = 15.44, T_9 = 3.84$.

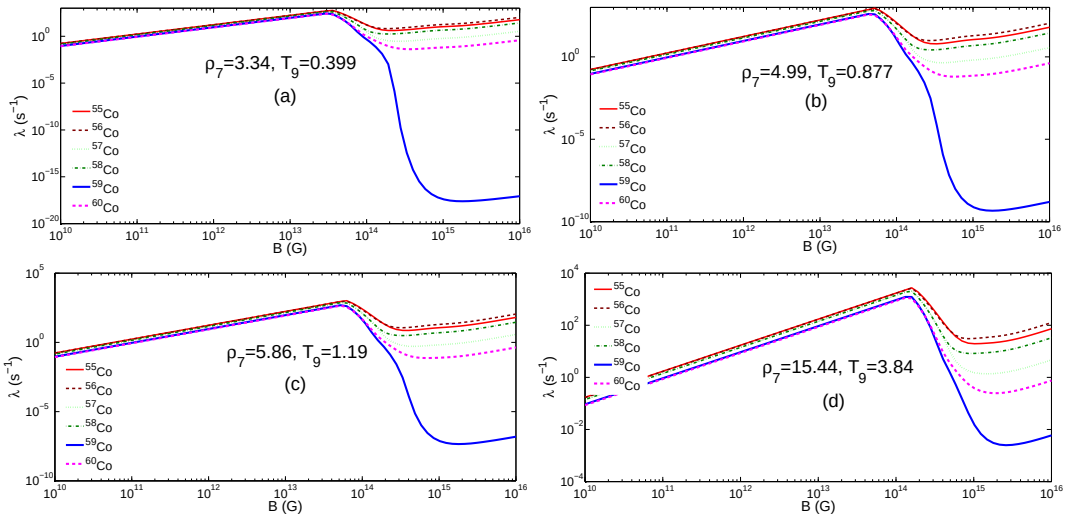

Fig. 2 The EC rates for $^{55-60}$ Co as a function of the magnetic field at $\rho_7 = 3.34, T_9 = 0.399$; $\rho_7 = 4.99, T_9 = 0.877$; $\rho_7 = 5.86, T_9 = 1.19$ and $\rho_7 = 15.44, T_9 = 3.84$.

Table 4 Comparisons of the maximum value of our calculations $\lambda_{\rm ec}^{B}({\rm LJ})$ with those of minimum value for some typical iron group nuclides in SMFs at $\rho_7 = 4010, Y_e = 0.41, T_9 = 7.33$ for $10^{13}{\rm G} \leq B \leq 10^{18}$ G.

	$\rho_7 = 4010, Y_e = 0.41, T_9 = 7.33$			
Nuclide	B	$\lambda_{\rm max}^{B}({\rm LJ})$	B	$\lambda_{\rm min}^{B}({\rm LJ})$
^{57}Mn	3.511e16	2.983e5	4.751e17	4.227e-2
^{58}Mn	3.511e16	1.998e5	4.751e17	2.654e-1
^{59}Mn	3.511e16	1.492e5	4.751e17	7.095e-4
^{60}Mn	3.511e16	1.496e5	4.751e17	8.283e-3
^{59}Fe	3.511e16	2.418e5	4.751e17	1.713e-2
^{60}Fe	3.511e16	1.522e5	4.751e17	1.759e-4
^{61}Fe	3.511e16	1.503e5	4.751e17	1.373e-3
^{56}Cr	3.511e16	2.101e5	4.751e17	6.943e-5
^{57}Cr	3.511e16	2.776e5	4.751e17	3.896e-4

the magnetic fields increase, U_F decreases greatly due to increase of electron Fermi energy. In an extremely strong magnetic field ($B \gg B_{\rm cr}$), the Landau column becomes a very long and very narrow cylinder along the magnetic field. According to Equations (11)–(17), when the magnetic field is constant, the electron chemical potential and electron energy will be strongly dependent on density. We select the magnetic field strength range to be $10^3 < B_{12} < 10^5$ G (e.g., $B_{12} = 10^3, 10^{3.5}, 10^4, 10^{4.5}$). According to Equations (7) and (8), we can ascertain that the electron chemical potential may be in the range $63.72 m_e c^2 < U_{\rm max}^{\rm B} < 116.6 m_e c^2$ for our model. For example, when $U_{\rm max}^{\rm B} = 80 m_e c^2$, the magnetic field strength B_{12} is $14.122593 \times 10^4, 7.0612965 \times 10^4, 4.7075313 \times 10^4$ for $\nu_{\rm max} = 1, 2, 3$, respectively. When $U_{\rm max}^{\rm B} = 100 m_e c^2$, the magnetic field strength B_{12} is $22.067793 \times 10^4, 11.0338965 \times 10^4, 7.355931 \times 10^4$ for $\nu_{\rm max} = 1, 2, 3$, respectively.

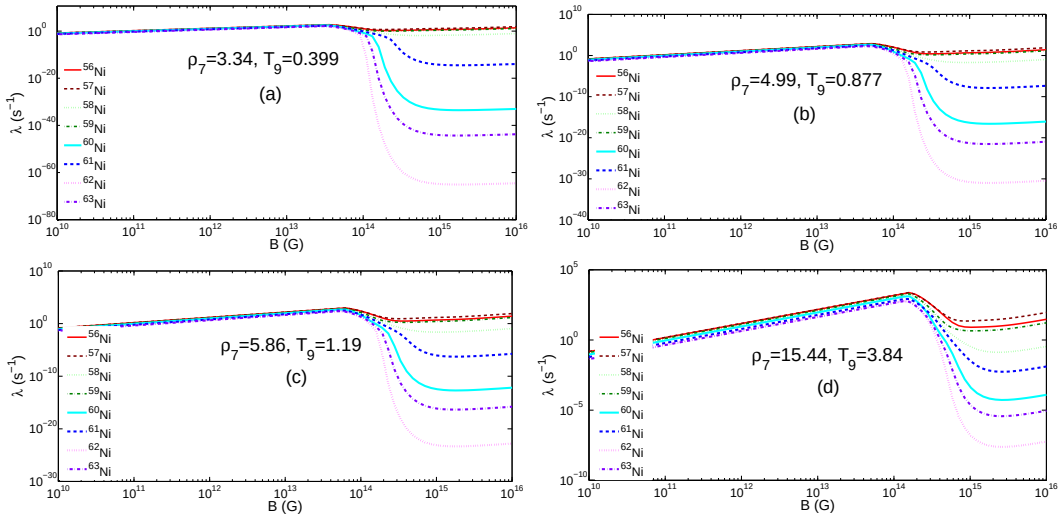

Fig. 3 The EC rates for $^{56-63}$ Ni as a function of the magnetic field at $\rho_7 = 3.34, T_9 = 0.399$; $\rho_7 = 4.99, T_9 = 0.877$; $\rho_7 = 5.86, T_9 = 1.19$ and $\rho_7 = 15.44, T_9 = 3.84$.

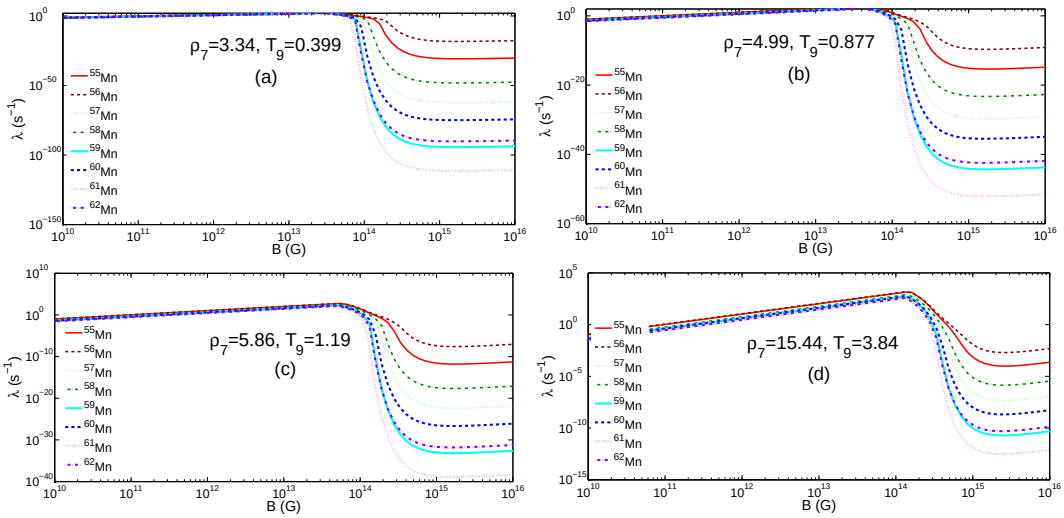

Fig. 4 The EC rates for $^{55-62}$ Mn as a function of the magnetic field at $\rho_7 = 3.34, T_9 = 0.399$; $\rho_7 = 4.99, T_9 = 0.877$; $\rho_7 = 5.86, T_9 = 1.19$ and $\rho_7 = 15.44, T_9 = 3.84$.

Based on the relativistic mean-field effective interactions NL3 (Lalazissis et al. 1997) and DD-ME2 (Lalazissis et al. 2005), following the works of Peña Arteaga et al. (2011), the influence of SMFs on the binding energy of nuclei is discussed. As the magnetic field increases, a mean parabolic increasing trend appears in terms of the binding energy per particle. For example, for ^{56}Fe, ^{78}Ni and ^{56}Co, the binding energy increases by 0.311 MeV, 0.632 MeV and 0.445 MeV, respectively when 10^{17} G $\sim$ 10^{18} G. The nuclear state will be more stable due to increase of nuclear binding energy. This is equivalent to significantly raising the threshold energy of the EC reaction. Therefore, the EC may be weakened.

The magnetic fields strongly effect electron phase space. Only axial symmetry is preserved, but the spherical symmetry is broken for the Dirac and Klein-Gordon equations (Peña Arteaga et al. 2011). From Figure 6, we find that the EC rates are influenced greatly when $T_9 > 1$ and $\rho_7 \geq 5.86$. For some iron group nuclei (e.g., $^{55-60}$ Co and $^{56-63}$Ni), the EC rates increase by three orders of magnitude when $B < 10^{14}$ G, then decrease and finally also increase as the SMFs increases. Such jumps show an obvious indication that the underlying shell structure may be changed in a fundamental way. Due to SMFs, these jumps in nuclear properties can be traced to the single-particle behavior. Due to these two levels having opposite angular momentum along the symmetry axis in SMFs, the nucleus becomes spin-polarized. Because of the increase in SMFs, the particle in a nucleus may move from a level going upwards and go to a level heading downward with increasing spin.

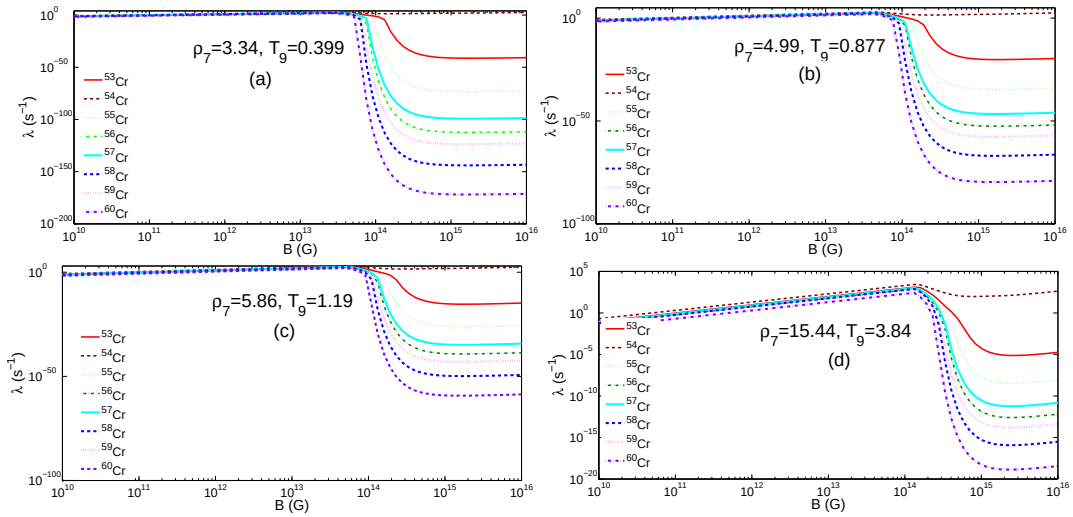

Fig. 5 The EC rates for $^{53-60}$Cr as a function of the electron chemical potential $\rho_7 = 3.34, T_9 = 0.399$; $\rho_7 = 4.99, T_9 = 0.877$; $\rho_7 = 5.86, T_9 = 1.19$ and $\rho_7 = 15.44, T_9 = 3.84$.

The EC and beta decay strongly determine the core entropy and electron-to-baryon ratio, and also influence the SCMWDs evolution. EC quickly reduces the number of electrons available for pressure support. In core-collapse supernovae and SCMWDs, the EC rates play a pivotal role. Tables 1-4 present our results at different typical astrophysical environments. We find the maximum value of the EC rates will get to $1.020 \times 10^3\,\mathrm{s}^{-1}$ at $B = 6.28 \times 10^{13}$ G for ^{55}Co, $1.869\times10^3\,\mathrm{s}^{-1}$ at $B = 1.322\times10^{14}$ G for ^{58}Co, $1.104 \times 10^4\,\mathrm{s}^{-1}$ at $B = 1.024 \times 10^{15}$ G for ^{56}Mn and $2.983 \times 10^5\,\mathrm{s}^{-1}$ at $B = 3.511 \times 10^{16}$ G for ^{57}Mn at $\rho_7 = 5.86, Y_e = 0.47, T_9 = 3.40$; $\rho_7 = 14.5, Y_e = 0.45, T_9 = 3.80$; $\rho_7 = 106, Y_e = 0.43, T_9 = 4.93$ and $\rho_7 = 4010, Y_e = 0.41, T_9 = 7.33$, respectively. On the other hand, the rates firstly increase and reach the maximum value, then may decrease more than three orders magnitude as the SMF increases (e.g. for ^{60}Ni at $\rho_7 = 5.86, Y_e = 0.47, T_9 = 3.40$).

The single-particle structure of nuclei for protons and neutrons will be strongly influenced by the SMFs. The nucleon paramagnetism will also be affected by the interaction between the magnetic field and the neutron (proton) magnetic dipole moment. The coupling of the orbital motion of protons with the magnetic field causes proton orbital magnetism. The interaction between the nucleus and SMF will remove all degeneracies in the single-particle spectrum. The SMF breaks the formerly degenerate levels with opposing signs of angular momentum projection. For example, figures 3 and 5 of Peña Arteaga et al. (2011) give a detailed discussion for ^{56}Fe. As the magnetic fields increase, the neutron and proton pairing gaps will be reduced by the single-particle energy splitting, and finally they will disappear.

Figures 6 displays the RCEA as a function of SMFs. Due to SMFs, the RCEA can decrease by more than three orders of magnitude when $B < 10^{14}$ G and $T_9 > 1$. The RCEA is very sensitive to SMFs in the EC process and when $10^{14}\,\mathrm{G} < \mathrm{B} < 10^{16}\,\mathrm{G}$, there are some changes by leaps and bounds then get to the maximum value due to quantum effects in SMFs. The main reason may arise from the fact that the EC rates are increased greatly due to the influence of density and SMFs. The electron chemical potential is strongly determined by the density and magnetic field according to Equations (7) and (11)–(19).

The convective instability of a magnetic WD's structure is caused by the heat released from thermonuclear reactions such as EC and beta decay under the influence of the SMF environment and neutrino cooling. As a WD with a strong, irregular magnetic field cools, convective instabilities may develop in different regions of the star at various times, giving rise in some cases to gamma-ray events.

The gamma-ray heating rates and neutrino energy loss by EC and beta decay play key roles in magnetic WD evolution. The neutrinos and antineutrinos are transparent to the WD's matter and will cool the core of the WD, while the gamma rays due to release of the EC will heat the stars. The evolutionary changes with the central density and the temperature of the magnetic core of the WD are determined by the competition among the contraction, cooling and heating processes. When the gamma ray is relatively fast enough to contract, the temperature becomes high enough to ignite Ne-O burning, which would result in formation of an Fe core. When cooling by neutrino energy loss is fast, the contraction leads to the collapse of the O-Ne-Mg core and an EC supernova. Thus the competitions between the heating rates by gamma ray and cooling rates by neutrino energy loss will strongly determine the fate of the instability of WDs.

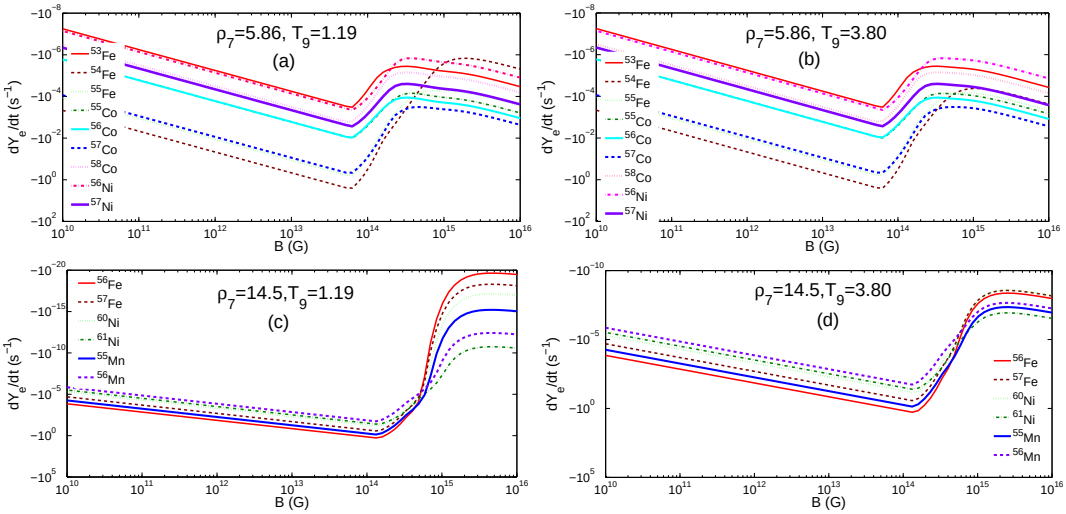

Fig. 6 The RCEA rates for some typical iron group nuclides as a function of the magnetic field at $\rho_7 = 5.86, 14.5$, $T_9 = 1.19, 3.80$.

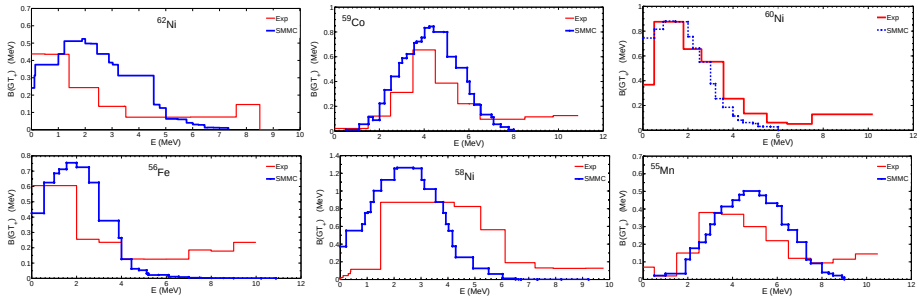

Fig. 7 The comparison of calculated B(GT_+) strength distribution against experiment (Alford et al. 1993; El-Kateb et al. 1994; Rapaport et al. 1984; Williams et al. 1995) for some typical iron group nuclei as a function of excitation energy in the corresponding daughter nuclei at temperature $T = 0.8$ MeV

Tables 5-8 display a comparison of our results for $\lambda_{\rm ec}^B$ (LJ)in SMFs with those of FFN ($\lambda_{\rm ec}^0$(FFN)), AUFD ($\lambda_{\rm ec}^0$ (AUFD)) and Nabi. For the case without SMFs, one finds that our results are in good agreement with AUFD's at relatively lower temperature and lower density (e.g. $\rho_7 = 5.86, T_9 = 3.40, Y_e = 0.47$). The rates of FFN are about one order of magnitude bigger than ours. Our results are also generally lower than those of Nabi at relatively high temperature and higher density (e.g., for ^{59,60}Mn, ^{60,61}Fe, ^{56}Cr at $\rho_7 = 4010, T_9 = 7.33, Y_e = 0.41$), but our results are larger than those of Nabi's by two orders magnitude for relatively lower temperature and lower density surroundings (e.g., for ^{54}Fe $\rho_7 = 5.86, T_9 = 3.40, Y_e = 0.47$). For the case with SMFs, due to SMF, our rates increase and even are larger by more than four orders of magnitude than those of FFN, AUFD and Nabi (e.g., $\rho_7 = 5.86, Y_e = 0.47, T_9 = 3.40$; $\rho_7 = 14.5, Y_e = 0.45, T_9 = 3.80$).

In this paper, the lattice energy may not be directly affected by SMFs. When we discuss the EC rates, we ignore the influence of SMFs on the lattice energy. On the other hand, due to the Coulomb forces acting as a perturbation to the magnetic forces (Garstang 1977), the magnetic influence on Zeeman splitting of atomic energy levels is not considered in SMFs.

We also neglect the effect of SMFs on the GT properties because the GT transition matrix elements may be independent of the magnetic fields (see the discussions from Fassio-Canuto (1969); Canuto & Ventura (1977) and references therein). Figure 7 features our results on the GT strength on iron group nuclei based on the pf-shell model. Some experimental data about GT distributions are also present in Alford et al. (1993); El-Kateb et al. (1994); Rapaport et al. (1984) and Williams et al. (1995). These experimental data are obtained from intermediate-energy charge exchange (n, p) or (p, n) cross sections. In order to account for the finite experimental resolution, our results for even-even nuclei (e.g., ^{56}Fe; ^{58,60,62}Ni) are smeared with Gaussians with standard deviation of 1.77 MeV from Figure 7. One can see that according to the SMMC approach, the renormalized B(GT_+) strengths for ^{56}Fe, ^{58,60,62}Ni are 2.682, 4.542, 3.510 and 2.410 MeV, respectively. From the experimental information, the B(GT_+) strengths are 2.601, 4.203, 3.200 and 2.600

Table 5 Comparisons of our calculations $\lambda_{\rm ec}^{B}({\rm LJ})$ in SMFs for some typical iron group nuclides with those of FFN's ($\lambda_{\rm ec}^{0}({\rm FFN})$) (Fuller et al. 1980; Fuller et al. 1982); AUFD's ($\lambda_{\rm ec}^{0}({\rm AUFD})$) (Aufderheide et al. 1990; AUFD), Nabi's ($\lambda_{\rm ec}^{0}({\rm Nabi})$) (NKK) and LJ's ($\lambda_{\rm ec}^{0}({\rm LJ})$), which are for the case without SMFs at $\rho_7 = 5.86, Y_e = 0.47, T_9 = 3.40$.

					$\lambda_{\rm ec}^{B}({\rm LJ})$			
Nuclide	$\lambda_{\rm ec}^{0}$(FFN)	$\lambda_{\rm ec}^{0}$(AUFD)	$\lambda_{\rm ec}^{0}$(Nabi)	$\lambda_{\rm ec}^{0}$(LJ)	$B_{12}=10$	$B_{12}=10^2$	$B_{12}=10^3$	$B_{12}=10^4$
^{56}Ni	1.30e-2	1.60e-2	4.83e-3	1.250e-2	1.479e2	1.663e2	3.946e0	2.733e1
^{57}Ni	9.93e-3	1.94e-2	4.76e-2	1.573e-2	1.478e2	1.628e2	1.195e1	8.383e1
^{58}Ni	3.72e-4	6.36e-4	7.31e-5	5.878e-4	1.099e2	6.049e1	4.347e-2	2.662e-1
^{59}Ni	4.31e-3	4.37e-3	1.32e-3	4.146e-3	1.242e2	8.072e1	2.152e0	1.524e1
^{60}Ni	9.17e-6	1.49e-6	1.70e-7	1.287e-6	8.943e1	2.098e1	6.090e-6	3.243e-5
^{53}Fe	3.91e-2	2.04e-2	5.08e-2	1.889e-2	1.162e2	6.429e1	1.068e1	6.736e1
^{54}Fe	2.95e-4	3.11e-4	3.07e-6	2.868e-4	1.160e2	4.631e1	1.065e-2	5.756e-2
^{55}Fe	1.57e-3	1.61e-3	1.47e-3	1.357e-3	1.203e2	4.630e1	7.350e-2	4.807e-1
^{55}Co	1.36e-1	1.41e-1	3.99e-2	1.336e-1	1.674e2	1.844e2	9.627e0	6.737e1
^{56}Co	6.91e-2	7.40e-2	1.14e-2	7.026e-2	1.639e2	1.626e2	1.647e1	1.166e2
^{57}Co	3.50e-3	1.89e-3	4.56e-4	7.026e-2	1.367e2	8.459e1	6.015e-1	4.212e0
^{58}Co	9.93e-3	1.94e-2	2.23e-4	1.680e-2	1.381e2	8.094e1	4.227e0	3.030e1

Table 6 Comparisons of our calculations of $\lambda_{\rm ec}^{B}({\rm LJ})$ in SMFs for some typical iron group nuclides with those of FFN's ($\lambda_{\rm ec}^{0}({\rm FFN})$); AUFD's ($\lambda_{\rm ec}^{0}({\rm AUFD})$), Nabi's ($\lambda_{\rm ec}^{0}({\rm Nabi})$) and LJ's ($\lambda_{\rm ec}^{0}({\rm LJ})$), which are for the case without SMFs at $\rho_7 = 14.5, Y_e = 0.45, T_9 = 3.80$.

					$\lambda_{\rm ec}^{B}({\rm LJ})$			
Nuclide	$\lambda_{\rm ec}^{0}$(FFN)	$\lambda_{\rm ec}^{0}$(AUFD)	$\lambda_{\rm ec}^{0}$(Nabi)	$\lambda_{\rm ec}^{0}$(LJ)	$B_{12}=10$	$B_{12}=10^2$	$B_{12}=10^3$	$B_{12}=10^4$
^{57}Co	1.04e-2	1.29e-2	2.40e-3	1.0123e-2	1.466e1	1.553e3	1.361e0	4.437e0
^{58}Co	1.55e-2	3.07e-2	1.55e-3	2.5604e-2	1.487e1	1.551e3	7.851e0	3.137e1
^{59}Co	5.44e-4	6.57e-4	2.09e-4	4.3564e-4	9.685e0	1.015e3	1.001e-2	5.302e-3
^{60}Co	1.15e-2	1.27e-2	1.74e-5	1.0012e-2	8.984e0	9.412e2	3.207e-1	5.986e-1
^{55}Mn	2.03e-5	2.25e-5	9.62e-6	2.1135e-5	1.086e1	1.138e3	3.945e-4	2.007e-4
^{56}Mn	4.29e-5	2.56e-4	2.42e-4	2.0552e-4	1.175e1	1.231e3	7.184e-3	4.299e-4
^{55}Fe	1.21e-2	6.20e-3	6.42e-3	5.7883e-3	1.290e1	1.351e3	3.206e-1	5.504e-1
^{56}Fe	2.81e-5	1.31e-6	7.14e-7	1.2452e-6	1.002e1	1.049e3	1.543e-5	6.894e-6
^{57}Fe	4.83e-5	1.84e-5	1.05e-5	1.6534e-5	1.023e1	1.071e3	6.382e-5	3.172e-5
^{60}Ni	1.39e-4	2.74e-5	3.23e-6	2.3372e-5	9.589e0	1.005e3	3.943e-4	1.063e-4
^{61}Ni	.....	1.20e-3	3.54e-4	1.0028e-3	1.336e1	1.400e3	2.089e-4	1.069e-2
^{53}Cr	1.63e-5	2.46e-6	8.85e-6	2.3225e-6	9.951e0	1.042e3	2.890e-5	1.498e-5

Table 7 Comparisons of our calculations of $\lambda_{\rm ec}^{B}({\rm LJ})$ in SMFs for some typical iron group nuclides with those of FFN's ($\lambda_{\rm ec}^{0}({\rm FFN})$); AUFD's ($\lambda_{\rm ec}^{0}({\rm AUFD})$), Nabi's ($\lambda_{\rm ec}^{0}({\rm Nabi})$) and LJ's ($\lambda_{\rm ec}^{0}({\rm LJ})$), which are for the case without SMFs at $\rho_7 = 106, Y_e = 0.43, T_9 = 4.93$.

					$\lambda_{\rm ec}^{B}({\rm LJ})$			
Nuclide	$\lambda_{\rm ec}^{0}$(FFN)	$\lambda_{\rm ec}^{0}$(AUFD)	$\lambda_{\rm ec}^{0}$(Nabi)	$\lambda_{\rm ec}^{0}$(LJ)	$B_{12}=10$	$B_{12}=10^2$	$B_{12}=10^3$	$B_{12}=10^4$
^{55}Mn	9.10e-3	8.73e-3	5.89e-3	7.8895e-3	1.013e2	1.138e3	1.059e4	5.686e-3
^{56}Mn	9.29e-3	2.90e-2	2.77e-2	2.6762e-2	1.096e2	1.231e3	1.104e4	5.788e-2
^{57}Mn	2.36e-5	4.03e-4	2.94e-4	3.8320e-4	8.300e1	9.323e2	7.641e3	1.577e-5
^{58}Mn	3.16e-4	2.94e-3	3.23e-4	2.8113e-4	5.561e1	6.246e2	4.813e3	1.959e-4
^{59}Fe	1.49e-4	1.83e-4	5.70e-4	2.4663e-5	6.729e1	7.558e2	6.426e3	3.307e-6
^{61}Ni	.....	5.07e-1	3.46e-2	3.3748e-1	5.935e1	6.687e2	6.236e3	1.319e-1
^{63}Ni	.....	3.87e-3	2.47e-3	2.5660e-3	4.262e1	4.787e2	4.275e3	4.367e-4

Table 8 Comparisons of our calculations of $\lambda_{\rm ec}^{B}({\rm LJ})$ in SMFs for some typical iron group nuclides with those of FFN's ($\lambda_{\rm ec}^{0}({\rm FFN})$); AUFD's ($\lambda_{\rm ec}^{0}({\rm AUFD})$), Nabi's ($\lambda_{\rm ec}^{0}({\rm Nabi})$) and LJ's ($\lambda_{\rm ec}^{0}({\rm LJ})$), which are for the case without SMFs at $\rho_7 = 4010, Y_e = 0.41, T_9 = 7.33$.

					$\lambda_{\rm ec}^{B}({\rm LJ})$			
Nuclide	$\lambda_{\rm ec}^{0}$(FFN)	$\lambda_{\rm ec}^{0}$(AUFD)	$\lambda_{\rm ec}^{0}$(Nabi)	$\lambda_{\rm ec}^{0}$(LJ)	$B_{12}=10^2$	$B_{12}=10^3$	$B_{12}=10^4$	$B_{12}=10^5$
^{57}Mn	4.29e2	8.36e2	3.41e2	7.6335e2	9.323e2	8.300e1	8.109e4	6.036e1
^{58}Mn	7.90e2	1.05e3	7.45e2	1.0326e3	6.246e2	5.561e1	5.433e4	1.672e2
^{59}Mn	.....	1.41e2	2.84e2	1.0132e2	4.679e2	4.166e1	4.070e4	1.972e1
^{60}Mn	.....	2.55e2	7.19e2	1.1876e2	4.667e2	4.163e1	4.080e4	8.100e0
^{59}Fe	7.43e2	7.20e2	2.70e2	6.1023e2	7.558e2	6.729e1	6.574e4	2.549e1
^{60}Fe	1.441e1	6.37e1	3.02e1	2.6867e1	4.667e2	4.235e1	4.090e4	5.071e-1
^{61}Fe	.....	1.63e2	2.41e2	1.4785e2	2.865e2	3.072e1	3.002e4	5.764e1
^{56}Cr	.....	3.33e1	2.95e1	2.8845e1	6.568e2	5.847e1	5.713e4	1.241e-1
^{57}Cr	.....	6.09e1	8.49e1	3.9436e1	7.206e2	7.727e1	7.549e4	5.071e-1

MeV for the same nuclei, respectively. In addition, our SMMC results for some odd-A nuclei (e.g., ^{59}Co, ^{55}Mn), from the (n, p) direction are also consistent with the experimental data (Alford et al. 1993; El-Kateb et al. 1994; Williams et al. 1995).

Based on the independent particle model, FFN parameterized the GT contribution in the process of discussions of the EC rates. FFN investigated the Q-value of the EC rates based on a semi-empirical atomic mass formula (Seeger & Howard 1975). Therefore, their results differed from ours. By using a simple calculation on the nuclear excitation level transitions, AUFD expanded FFN's works and analyzed the nuclear excitation level. Their method may be a little rough. Only the low angular momentum states around the GT transitions are considered and the nuclear excitation energy distribution is analyzed according to the pn-QRPA theory by Nabi. In this paper, we compute an average of the GT intensity distribution by applying the method of SMMC. Our calculations are in good agreement with experiments. However, our results for some odd-A nuclides may be biased generally small.

Based on the above discussions, the change of EC rate affects the rate of thermonuclear reaction, and the evolution and stability of SCMWDs. The change of EC rate also affects the change of electron abundance, and the change of electron degenerate pressure and entropy. The EC rates also influence the burning and cooling in the process WDs evolution, and finally determine the fate of WDs. For the mass variation of the SCMWDs, we believe that it may be related to accretion of the SCMWDs, stellar wind, convection and other factors, therefore, we did not consider the effect of the change of EC rate on the mass of SCMWDs.

On the other hand, during the evolution of SCMWDs, the hydrostatic equilibrium of the material will affect the density distribution of the SCMWDs and the equation of state of the material. Density changes will strongly affect the electronic Fermi energy. The higher the density, the larger the Fermi level becomes. However, the increase of SMFs reduces the chemical potential of electronic gases, and eventually will weaken EC thermonuclear reaction. At the same time, the increase of temperature accelerates the speed of electron movement, and leads to electronic kinetic energy increasing greatly. To some extent, this will weaken the effect of magnetic field on EC.

Soft gamma-ray repeaters (SGRs) and anomalous X-ray pulsars (AXPs) can be explained as recently proposed highly magnetized WDs. Some interesting behaviors such as a wide array of X-ray activity including short bursts, large outbursts, giant flares, quasi-periodic oscillations, enhanced spin-down, glitches and anti-glitches appear in magnetars and are discussed by Kaspi & Beloborodov (2017). The observations show that persistent X-ray emission of a magnetar such as magnetic WDs could originate from magnetic field decay or heating from magnetospheric current and/or from the EC reaction in the crust.

5 CONCLUSIONS

In this paper, focusing on the electronic structure and the properties of matter, we discuss the EC process in detail in SCMWDs. When we ignore the effect of SMFs on EC, one finds that our results are in good agreement with AUFD's at relatively lower temperature and lower density (e.g. $\rho_7 = 5.86, T_9 = 3.40, Y_e = 0.47$). The rates of FFN are bigger by about one order magnitude than ours. Nabi's results are generally larger than ours at relatively higher density (e.g., for ^{59,60}Mn, ^{60,61}Fe, ^{56}Cr at $\rho_7 = 4010, T_9 = 7.33, Y_e = 0.41$), but are smaller by two orders magnitude than ours for relatively lower density (e.g. for ^{54}Fe $\rho_7 = 5.86, T_9 = 3.40, Y_e = 0.47$). When we take the effect of SMFs on EC into account, our rates are higher by about four orders of magnitude than those of FFN, AUFD and Nabi.

SCMWDs represent an important object in current astrophysical research, which may be helpful and significant to explain many astronomical phenomena. We attempt to study the EC thermonuclear reaction in a strong magnetic field of SCMWDs in order to understand the nature of SCMWDs. However, uncertainties in the internal equation of state for SCMWDs, the physical mechanisms of the strong magnetic field formed and all kinds of complex influences of thermonuclear reaction, the thermal evolution, magnetic evolution and cooling mechanism of SCMWDs are very challenging and complex problems. The rationality and scientific nature and feasibility for a variety of SCMWD theoretical models and mechanisms need to be continuously explored in our future works. For example, what observations from the SCMWDs can help judge the rationality and science of the results obtained by different methods? How can the relevant observational characteristics and data from the radio band be closely combined with the theory and be constantly improved to make its analysis reasonable? These will be very challenging and interesting issues for us to continue to explore and study.

Acknowledgements This work was supported in part by the National Natural Science Foundation of China (Grant Nos. 11965010 and 11565020), the Natural Science Foundation of Hainan Province (Grant Nos. 2019RC239, 118MS071 and 114012), the Counterpart Foundation of Sanya (Grant 2016PT43 and 2019PT76), the Special Foundation of Science and Technology Cooperation for Advanced Academy and Regional of Sanya (Grant 2016YD28) and the Scientific Research Starting Foundation for 515 Talented Project of Hainan Tropical Ocean University (Grant RHDRC201701).

References

Alford, W. P., Brown, B. A., Burzynski, S., et al. 1993, Phys. Rev. C, 48, 2818

Aufderheide, M. B., Brown, G. E., Kuo, T. T. S., et al. 1990, ApJ, 362, 241

Aufderheide, M. B., Fushiki, I., Woosley, S. E., & Hartmann, D. H. 1994, ApJS, 91, 389

Bjorken, J. D., Drell, S. D., & Mansfield, J. E. 1965, Physics Today, 18, 81

Blinnikov, S. I., Dunina-Barkovskaya, N. V., & Nadyozhin, D. K. 1996, ApJS, 106, 171

Canuto, V., & Ventura, J. 1977, Fund. Cosmic Phys., 2, 203

Chamel, N., Fantina, A. F., & Davis, P. J. 2013, Phys. Rev. D, 88, 081301

Chandrasekhar, S. 1935, MNRAS, 95, 207

Dai, Z., Lu, T., & Peng, Q. 1993, A&A, 272, 705

Das, U., & Mukhopadhyay, B. 2012a, Phys. Rev. D, 86, 042001

Das, U., & Mukhopadhyay, B. 2012b, International Journal of Modern Physics D, 21, 1242001

Das, U., & Mukhopadhyay, B. 2013, Phys. Rev. Lett., 110, 071102

Das, U., Mukhopadhyay, B., & Rao, A. R. 2013, ApJL, 767, L14

Dean, D. J., Langanke, K., Chatterjee, L., et al. 1998, Phys. Rev. C, 58, 536

El-Kateb, S., Jackson, K. P., Alford, W. P., et al. 1994, Phys. Rev. C, 49, 3128

Fassio-Canuto, L. 1969, Physical Review, 187, 2141

Fuller, G. M., Fowler, W. A., & Newman, M. J. 1980, ApJS, 42, 447

Fuller, G. M., Fowler, W. A., & Newman, M. J. 1982, ApJ, 252, 715

Fuller, G. M., Fowler, W. A., & Newman, M. J. 1985, ApJ, 293, 1

Gambhir, Y. K., Ring, P., & Thimet, A. 1990, Annals of Physics, 198, 132

Gao, Z. F., Shan, H., Wang, W., & Wang, N. 2017, Astronomische Nachrichten, 338, 1066

Gao, Z. F., Wang, N., Xu, Y., et al. 2015, Astronomische Nachrichten, 336, 866

Gao, Z. F., Wang, N., Yuan, J. P., et al. 2011, Ap&SS, 332, 129

Garstang, R. H. 1977, Reports on Progress in Physics, 40, 105

Girifalco, L. A. 1973, Statistical physics of materials (New York: Wiley-Interscience)

Juodagalvis, A., Langanke, K., Hix, W. R., Martínez-Pinedo, G., & Sampaio, J. M. 2010, Nucl. Phys. A, 848, 454

Kaspi, V. M., & Beloborodov, A. M. 2017, ARA&A, 55, 261

Kemp, J. C., Swedlund, J. B., Landstreet, J. D., & Angel, J. R. P. 1970, ApJL, 161, L77

Kundu, A., & Mukhopadhyay, B. 2012, Modern Physics Letters A, 27, 1250084

Lai, D. 2001, Reviews of Modern Physics, 73, 629

Lai, D., & Shapiro, S. L. 1991, ApJ, 383, 745

Lalazissis, G. A., König, J., & Ring, P. 1997, Phys. Rev. C, 55, 540

Lalazissis, G. A., Nikšić, T., Vretenar, D., & Ring, P. 2005, Phys. Rev. C, 71, 024312

Langanke, K., & Martinez-Pinedo, G. 1998, Physics Letters B, 436, 19

Langanke, K., & Martínez-Pinedo, G. 2000, Nucl. Phys. A, 673, 481

Li, X. H., Gao, Z. F., Li, X. D., et al. 2016, International Journal of Modern Physics D, 25, 1650002

Liu, J.-J. 2013, MNRAS, 433, 1108

Liu, J.-J. 2014, MNRAS, 438, 930

Liu, J.-J. 2016, RAA (Research in Astronomy and Astrophysics), 16, 83

Liu, J.-J., & Gu, W.-M. 2016, ApJS, 224, 29

Liu, J.-J., Kang, X.-P., Hao, L.-H., et al. 2016, RAA (Research in Astronomy and Astrophysics), 16, 174

Liu, J.-J., & Liu, D.-M. 2016, Ap&SS, 361, 246

Liu, J.-J., & Liu, D.-M. 2018a, European Physical Journal C, 78, 84

Liu, J.-J., & Liu, D.-M. 2018b, RAA (Research in Astronomy and Astrophysics), 18, 008

Liu, J.-J., Peng, Q.-H., Hao, L.-H., et al. 2017a, RAA (Research in Astronomy and Astrophysics), 17, 107

Liu, J.-J., Peng, Q.-H., & Liu, D.-M. 2017b, Chinese Physics C, 41, 095101

Luo, Z.-Q., & Peng, Q.-H. 1997, Chinese Astronomy and Astrophysics, 21, 254

Maeda, K., Kawabata, K., Li, W., et al. 2009, ApJ, 690, 1745

Nabi, J. U., & Klapdor-Kleingrothaus, H. V. 1999, arXiv e-prints, nucl

Peña Arteaga, D., Grasso, M., Khan, E., & Ring, P. 2011, Phys. Rev. C, 84, 045806

Potekhin, A. Y., & Chabrier, G. 2013, A&A, 550, A43

Potekhin, A. Y., & Chabrier, G. 2018, A&A, 609, A74

Potekhin, A. Y., Fantina, A. F., Chamel, N., et al. 2013, A&A, 560, A48

Rapaport, J., Alarcon, R., Brown, B. A., et al. 1984, Nucl. Phys. A, 427, 332

Reimers, D., Jordan, S., Koester, D., et al. 1996, A&A, 311, 572

Scalzo, R. A., Aldering, G., Antilogus, P., et al. 2010, ApJ, 713, 1073

Schmidt, G. D., & Smith, P. S. 1995, ApJ, 448, 305

Seeger, P. A., & Howard, W. M. 1975, Nucl. Phys. A, 238, 491

Shapiro, S. L., & Teukolsky, S. A. 1983, Black Holes, White Dwarfs, and Neutron Stars: the Physics of Compact Objects (A Wiley-Interscience Publication, New York: Wiley)

Vretenar, D., Afanasjev, A. V., Lalazissis, G. A., & Ring, P. 2005, Phys. Rep., 409, 101

Williams, A. L., Alford, W. P., Brash, E., et al. 1995, Phys. Rev. C, 51, 1144